ADVANCED FUNCTIONAL MATERIALS
www.afm-journal.de

Thymus Extracellular Matrix-Derived Scaffolds Support Graft-Resident Thymopoiesis and Long-Term In Vitro Culture of Adult Thymic Epithelial Cells

M. Adelaide Asnaghi, Thomas Barthlott, Fabiana Gullotta, Valentina Strusi, Anna Amovilli, Katrin Hafen, Gitika Srivastava, Philipp Oertle, Roberto Toni, David Wendt, Georg A. Holländer, and Ivan Martin**

The thymus provides the physiological microenvironment critical for the development of T lymphocytes, the cells that orchestrate the adaptive immune system to generate an antigen-specific response. A diverse population of stroma cells provides surface-bound and soluble molecules that orchestrate the intrathymic maturation and selection of developing T cells. Forming an intricate 3D architecture, thymic epithelial cells (TEC) represent the most abundant and important constituent of the thymic stroma. Effective models for in and ex vivo use of adult TEC are still wanting, limiting the engineering of functional thymic organoids and the understanding of the development of a competent immune system. Here a 3D scaffold is developed based on decellularized thymic tissue capable of supporting in vitro and in vivo thymopoiesis by both fetal and adult TEC. For the first time, direct evidences of feasibility for sustained graft-resident T-cell development using adult TEC as input are provided. Moreover, the scaffold supports prolonged in vitro culture of adult TEC, with a retained expression of the master regulator Foxn1. The success of engineering a thymic scaffold that sustains adult TEC function provides unprecedented opportunities to investigate thymus development and physiology and to design and implement novel strategies for thymus replacement therapies.

1. Introduction

The thymus constitutes the primary lymphoid organ for the formation of functionally competent T cells derived from blood-borne precursors.[1] This process is critically dependent on physical and functional interactions of maturing T cells (thymocytes) with a range of thymic stromal cells. The most abundant stromal cells are thymic epithelial cells (TEC), which are classified based on their positional, structural, antigenic, and functional characteristics either as cortical (cTEC) or as medullary epithelia (mTEC). TEC themselves and the interaction with their cell surface and secreted molecules are critical for the homing of blood-borne precursors, their lineage-commitment, subsequent survival, expansion, maturation and selection to functionally competent T cells.[2–4]

Dr. M. A. Asnaghi, Dr. F. Gullotta, Dr. V. Strusi, A. Amovilli, Dr. D. Wendt, Prof. I. Martin
Department of Biomedicine
University Hospital Basel
University of Basel
Basel 4031, Switzerland
E-mail: ivan.martin@usb.ch

Dr. T. Barthlott, K. Hafen, Prof. G. A. Holländer
Department of Biomedicine
University Children's Hospital
University of Basel
Basel 4058, Switzerland
E-mail: georg-a.hollaender@unibas.ch

The ORCID identification number(s) for the author(s) of this article can be found under https://doi.org/10.1002/adfm.202010747.

DOI: 10.1002/adfm.202010747

Dr. G. Srivastava, Dr. P. Oertle
ARTIDIS AG
Basel 4057, Switzerland

Dr. P. Oertle
Biozentrum and the Swiss Nanoscience Institute
University of Basel
Basel 4056, Switzerland

Prof. R. Toni
Department of Medicine and Surgery – DIMEC, Unit of Biomedical Biotechnological and Translational Sciences (S.BI.BI.T.)
Laboratory of Regenerative Morphology and Bioartificial Structures (Re.Mo.Bio.S.)
University of Parma
Parma 43121, Italy

Prof. R. Toni
Division of Endocrinology
Diabetes, and Metabolism
Tufts Medical Center – Tufts University School of Medicine
Boston, MA 02111, USA

Human thymus involution begins after the first year of life, results in a lower T cell output as a function of age and, consequently, contributes to immunosenescence.[5] This state is marked in peripheral lymphoid tissues by the accumulation of T cells that are functionally impaired and that display at the population level a reduced TCR repertoire. Immunosenescence has been related to an increased risk for autoimmunity and cancer.[6,7] Thymus cellularity and function are susceptible to different exogenous influences such as the exposure to cytokines in the context of infections, corticosteroids as a consequence of stress, and chemo-radiotherapy for cancer treatment.[8–10] Consequently, there is a transient or, at times, even complete loss of thymus function that correlates with a quantitative and qualitative TEC impairment and results in a delayed repopulation of a numerically and functionally normal peripheral T-cell compartment. This deficiency correlates with an increased susceptibility for potentially life-threatening infections and tumor relapse.[11] Strategies to the regeneration of the TEC compartment based on cytokine and growth factor treatments have so far not only remained limited in effect and outcome but are also marred by undesirable side effects.[12] Hence, alternative approaches are warranted that accelerate thymus recovery following injury or rejuvenate thymus function in the context of aging.

A detailed understanding of the molecular and cellular mechanisms operational in establishing and maintaining a functional TEC-scaffold construct able to be populated with hematopoietic cells will undoubtedly aid in meeting such an aspiring goal. However, suitable and informative experimental models that support the ex vivo culture of functionally competent adult TEC are currently lacking.

TEC characteristically exerts their function organized as a continuous 3D cellular network throughout the organ. When grown independent of such a complex architecture, TEC quickly loses their competence to support thymopoiesis which is paralleled by a loss of molecules known to be critical for TEC proliferation, differentiation, and function—including the master regulator FOXN1.[13–16] Intact fetal thymus lobes (so called fetal thymic organ cultures, FTOC) or the aggregation of selected, isolated fetal thymic stromal cells (designated reaggregate thymic organ culture, RTOC) have been used to manipulate TEC in vitro and to study their functional competence.[17] However, due to size restrictions and the requirement of fetal cellular input, both models have their inherent limitations restricting their utility for detailed molecular studies of the postnatal thymus and exploitation for organ replacement strategies. Moreover, the use of postnatal TEC precludes the formation of 3D aggregates and the modeling of an adult thymus microenvironment.[18]

Prof. G. A. Holländer
Developmental Immunology
Department of Paediatrics and Weatherall Institute
of Molecular Medicine
University of Oxford
Oxford OX3 9DS, UK
E-mail: georg.hollander@paediatrics.ox.ac.uk
Prof. I. Martin
Department of Biomedical Engineering
University Hospital Basel
University of Basel
Allschwil 4123, Switzerland

Attention has thus turned to the emerging field of immune organ engineering and the use of biomaterials that foster the formation and manipulation of functional 3D tissue architectures employing controlled chemophysical culture conditions that better recapitulate the native microenvironment.[19,20] Initial attempts of TEC grown on CellFoam biomatrices have demonstrated an enhanced T-cell production when compared to monolayer cultures.[21] Hydrogels employed in combination with a 3D scaffold (i.e., nonwoven fibrous mesh of Jettex 2005/45) preserved key features of medullary TEC grown in vitro for 14 d.[22] Hydrogels alone maintained the molecular and functional properties of TEC in mini thymic units; however, in vivo thymopoiesis was skewed to the CD8 lineage and peripheral T cell numbers did not increase over time, suggesting that thymopoiesis was not sustained. Furthermore, the lack of congenic markers to discriminate between contaminating donor T cells present in the TEC preparation at the time of grafting and host bone-marrow-derived, de novo generated T cells challenges interpretation of these results.[23] Recently, collagen I was used to produce scaffolds in an attempt to mimic the thymic extracellular matrix (ECM) microstructure.[24] These scaffolds sustained TEC survival, but failed to support thymopoiesis when grafted in vivo. Although these methods did provide a 3D environment closer to the organ's physiological architecture, none could robustly support lasting thymopoiesis—likely because the resultant microenvironments lacked the complex molecular cues conveyed by the native thymic ECM.

Numerous tissues and organs have been decellularized in vitro via a wide variety of physical, chemical, and enzymatic methods with the ultimate aim of reproducing the ECM microenvironment of a particular biological compartment. Recently, decellularized thymic tissue has been used in combination with fetal or neonatal TEC to generate thymic organoids.[25,26] Although without direct evidence of graft-resident ongoing thymopoiesis, these studies suggest the opportunity to exploit the native thymus ECM to support functional TEC in vitro and in vivo.

We hypothesize here that 3D scaffolds generated from decellularized thymic tissue can support ex vivo culture and in vivo thymopoietic capacity of adult TEC. As compared to decellularized whole organs, highly interconnected porous scaffolds would favor more efficient cell colonization, possibly leading to improved cell to cell interactions. Our findings demonstrate that the developed scaffold can preserve the thymopoietic competence of adult TEC.

2. Results

2.1. Bioreactor-Based Decellularization of Murine Thymi Efficiently Removes Cells and DNA, Preserving ECM Composition

Thymi were harvested from 4 to 6 weeks old mice and exposed to a decellularization process over a 6 day course in a perfusion bioreactor (**Figure 1**A). The protocol used a combination of hypotonic stress to allow for complete cell lysis, enzymes to remove DNA residues and shear stresses to favor cell detachment as well as efficient removal of cell debris. As a result, thymic lobes turned white and translucent (Figure 1B, left panels). Hematoxylin & eosin staining on tissue sections

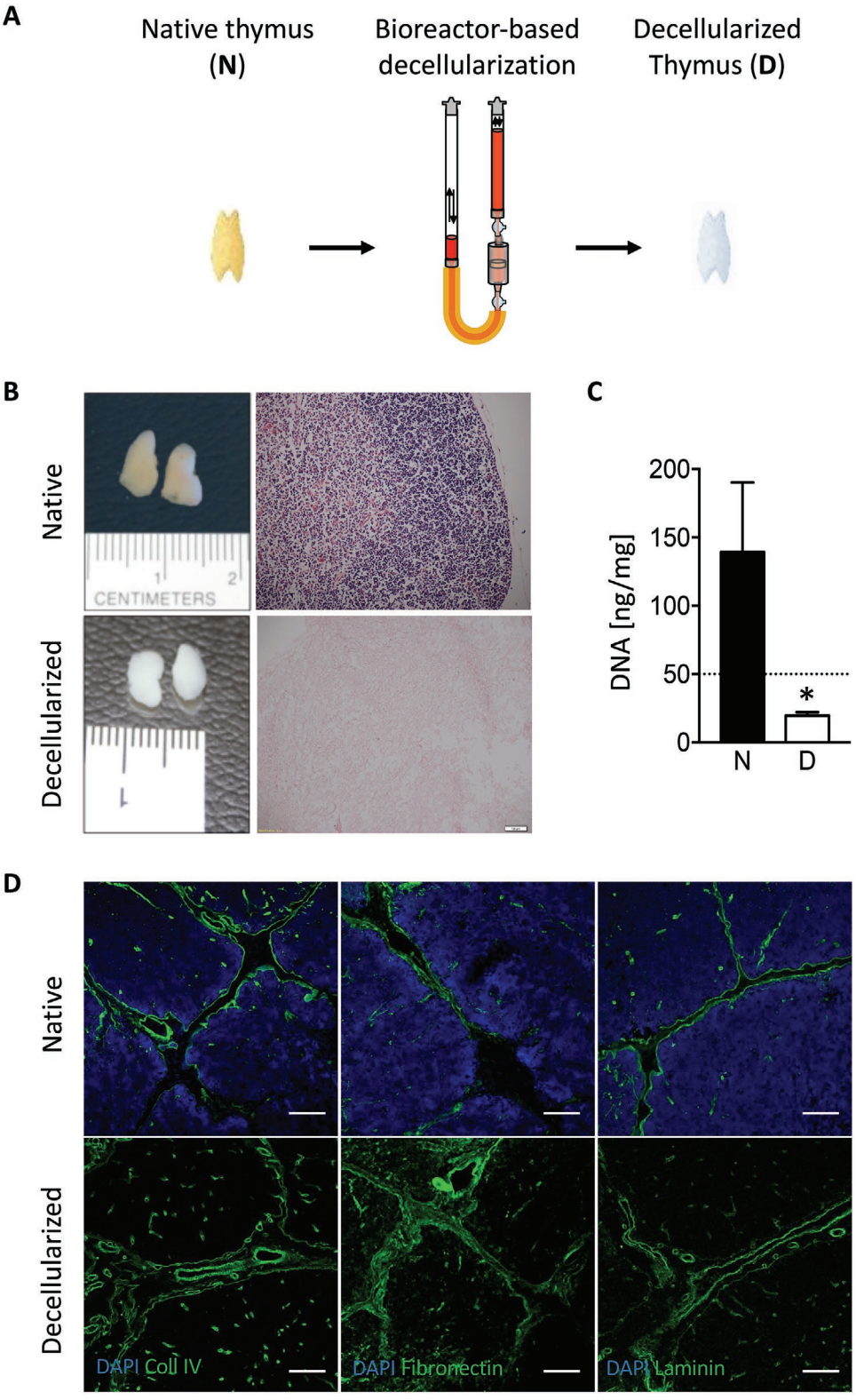

Figure 1. Decellularization of murine thymus in perfusion bioreactor allows efficient removal of cells and nuclear matter, while preserving extracellular matrix proteins. A) Murine thymi were decellularized in a perfusion bioreactor. B) Photographs and representative images of hematoxylin and eosin-stained sections of thymic lobes before and after the decellularization process. Scale bar: 500 µm. C) Quantification of DNA content by Picogreen assay in native (N) and decellularized (D) thymi. D) Immunofluorescence staining for collagen IV, fibronectin, and laminin in native and decellularized tissue (green). Nuclei were stained by DAPI (blue).

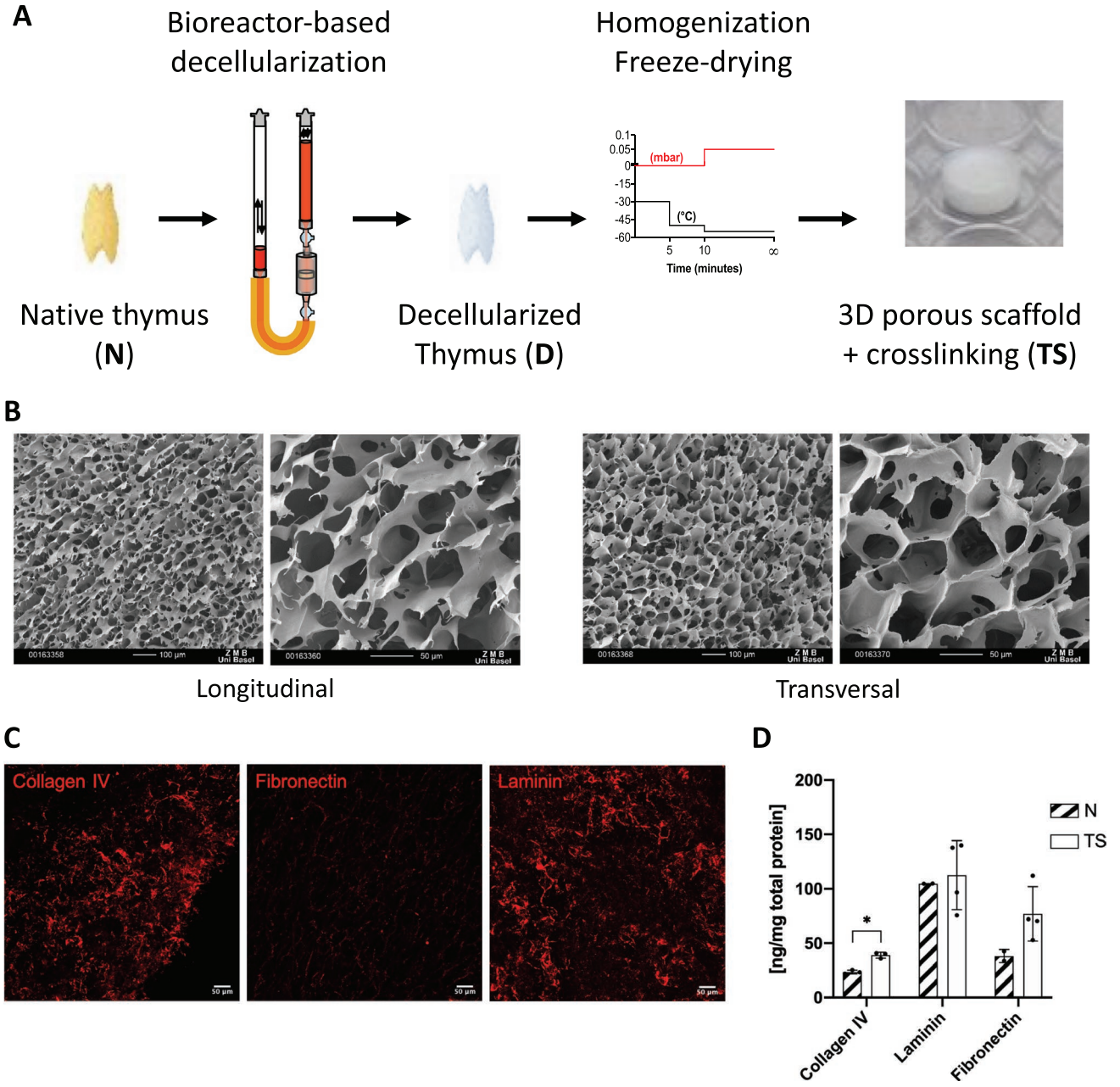

Figure 2. Use of decellularized murine thymus for the production of 3D porous scaffolds with preserved ECM composition. A) Schematic representation of the 3D scaffold production process. B) Scanning electron microscopy images of longitudinal and transversal sections of the 3D thymus scaffold (TS). C) Immunofluorescence staining for collagen IV, fibronectin, and laminin in TS. Scale bar: 50 µm. D) Quantification of collagen IV, laminin, and fibronectin in native thymus (N) and 3D thymus scaffold (TS). Data are normalized over the total protein content.

demonstrated a complete absence of intact cells and a lack of nuclei in the treated samples (Figure 1B, right panels). The DNA content of decellularized thymic lobes was significantly reduced when compared to untreated tissue (Figure 1C), well below the reported threshold for sufficient ECM decellularization (residual DNA < 50 ng dsDNA per mg ECM dry tissue).[27] The ECM maintained its native architecture and composition as characterized by immunofluorescence staining for collagen IV, fibronectin, and laminin (Figure 1D). These analyses confirmed the suitability of the protocol for efficient decellularization and preservation of the main native ECM components.

2.2. 3D Scaffolds Based on Decellularized Thymus

Decellularized thymi were homogenized and 3D porous thymus scaffolds (TS) were produced by freeze-drying technique. The stability of TS was improved by crosslinking to allow for easier manipulations and longer degradation times for in vitro and in vivo studies (**Figure 2**A). As displayed in SEM micrographs, the resultant TS morphology was characterized by a highly homogeneous structure of well-interconnected pores known to favor cell seeding and proper mass transport of nutrients and waste products throughout the scaffold volume

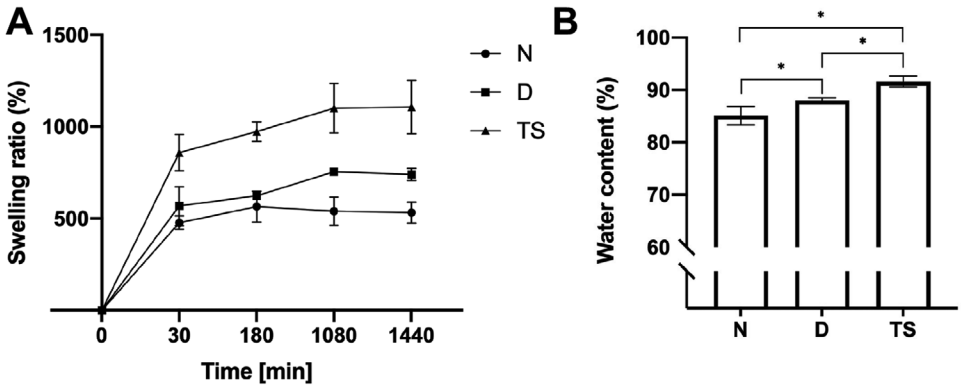

Figure 3. Physical characterization of 3D thymus scaffold (TS) in comparison to native (N) and decellularized (D) thymus: A) swelling ratio over time and B) water content at equilibrium.

(Figure 2B). Immunofluorescence analyses furthermore revealed that TS contained all three main components of the native ECM (Figure 2C), suggesting limited protein depletion as a consequence of scaffold production process. Protein quantification confirmed preservation of the native ECM, with the similar protein content of laminin and fibronectin, and a significant enrichment in collagen IV in TS versus native thymus (Figure 2D). Overall, the method allowed the facile fabrication of 3D scaffolds with a reproducible microstructure in a composition comparable to that of native thymus ECM.

The results of swelling tests are shown in **Figure 3**A. The weight of all samples increased rapidly in the first 30 min of immersion, with the scaffolds reporting the highest increase. While native tissues reached a plateau already after 3 h, the weight of decellularized tissues and TS kept increasing up to 18 h. Overall, TS showed the highest swelling ability, up to two times the swelling ratio of native thymi. At equilibrium, 24 h after immersion in PBS, the percentage of water content was estimated (Figure 3B). Water content progressively increased from native thymi (85.13 ± 1.75) to decellularized tissues (87.99 ± 0.55) to TS (91.62 ±1.02), likely due to the hydrophilic properties of the ECM and the more favorable microstructure.

The nanomechanical properties of the native thymus, decellularized tissue, and 3D thymus scaffolds were characterized by atomic force microscopy (AFM). All three groups showed elastic modulus values typical of ECM and cellular components.[28–33] The elastic modulus was increased in decellularized (22 ± 18 kPa) versus native (12 ± 6 kPa) tissue, with no significant difference (**Figure 4**B). This reflects the effective removal of cells and debris—with the stiffer ECM being thus exposed and directly measured during the analysis. This observation is also confirmed by the local force maps, which visualize the spatial distribution of nanomechanical properties at μm resolution (Figure 4C–F). The force maps of native samples revealed a recurrent pattern possibly associated with the cell compartment (Figure 4C). Such preferential pattern was lost in the force maps of decellularized samples, indicative of the efficient removal of the cell component (Figure 4D). The cumulative histograms in Figure 4G–J provide a closer view on the distribution of values within one tissue sample or scaffold. The histogram of the native thymus was characterized by a distinct peak at 3 kPa and a marked drop of stiffer values (Figure 4G). In contrast, the peak of the decellularized sample was broader and shifted around 5.5 kPa, with a much larger contribution of stiff values typical for ECM components (Figure 4H)—corroborating the removal of cells and debris during the decellularization process. On average, thymus scaffolds were characterized by a significant increase in elastic modulus (116 ± 77 kPa), as compared to both native and decellularized samples (Figure 4B). Recorded values were in the range of native basement membranes,[30,31] demonstrating that the process of scaffold fabrication allowed the preservation of nanomechanical properties typical of native ECM. The increased elastic modulus of TS may be directly related to the dissociation of the native ECM into individual components, which often results in mechanical properties different from the original compound.[34] High variability in elastic modulus was observed in the TS group, with some samples having much higher elastic modulus than N and D, and other samples having values comparable to the other groups. The force maps of the softest and the stiffest TS are displayed in Figure 4E,F. Both force maps were marked by a distinct pattern of stiff networks seemingly filled with patches of softer material. Distinctly, the stiffer components take up a larger area in the stiff TS as compared to the softer TS. The histogram of the soft TS showed a peak at low values and a rather narrow distribution towards higher moduli (Figure 4I), consistent with the stiffer components also visible in the force maps. The cumulative histogram for the stiff TS was shifted toward higher values, lacking a soft component and having a broad distribution of modulus values (Figure 4J), also reflecting the heterogeneity observed in the force maps. Overall, the performed AFM analyses revealed nanomechanical properties typical of native ECM arranged in a scaffold-specific ultrastructure.

2.3. TS Seeded with Fetal TEC Supports Extended T Cell Development

TS was next seeded with a suspension of thymic stroma cells and thymocytes recovered from embryonic day 14.5 (E14.5) thymic lobes treated with collagenase. At this developmental stage, thymocytes lack the expression of the coreceptors CD4 and CD8 (a cell phenotype designated double negative, DN) and acquire the expression of these cell surface markers only

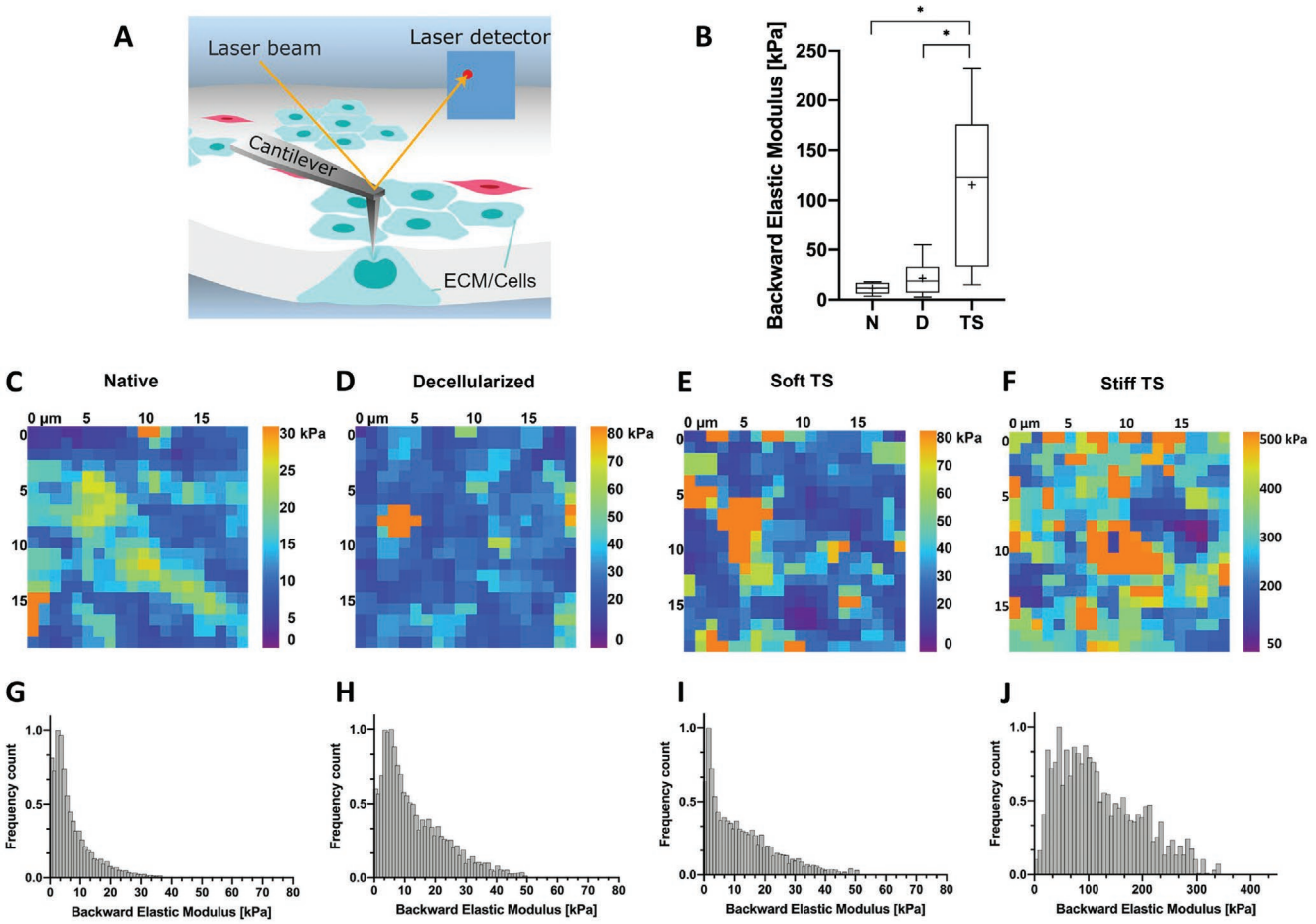

Figure 4. Nanomechanical characterization of native thymus (N), decellularized tissue (D), and 3D thymus scaffold (TS). A) Schematic representation of the atomic force microscopy working principle (modified with permission from Asgeirsson et al.).[35] B) Comparison of backward elastic modulus. C–F) Representative force maps and G–J) elastic modulus distribution from each group, including a soft and a stiff TS.

after functional engagement with a normal thymus environment. The cell surface detection of CD4 and CD8 thus indicates the functional competence of the thymus stroma to direct an important transition in thymopoiesis. Reconstituted TS were compared to RTOC which are generated by placing a small volume of a concentrated cell slurry (1–2 µL) on floating permeable filters to form within hours a firm thymus organoid. In addition, decellularized thymic tissue that had not been subjected to freeze/dry cycles was also seeded with a combination of E14.5 thymus stromal cells and thymocytes (**Figure 5**A). After 5 d of culture, RTOC, seeded TS and decellularized thymus tissue were mechanically dissociated and cells were analyzed for their expression of CD4 and CD8 (Figure 5B). TS repopulated with E14.5 thymic stroma cells and thymocytes supported the generation of double positive (DP, i.e., $CD4^{pos}$ and $CD8^{pos}$) cells comparable to the frequency of these cells found in RTOC. In contrast, the seeding of decellularized thymic tissue was very restricted and, consequently, only few thymocytes could be recovered, without a clear DP phenotype. The seeding of decellularized thymus tissue by injection has indeed proven particularly challenging in our hands in independent experiments and did neither generate nor maintain DP/SP thymocytes. Hence, only TS was used in further investigations, able to support the establishment of a functional thymic microenvironment capable of supporting the development of DN thymocytes to DP cells.

We next probed in a proof of principle experiment whether reconstituted TS grafted into athymic nude mice could attract hematopoietic precursors of the host and support thymopoiesis over an extended period of time. To distinguish cells according to their origin, the transplants were seeded with DN thymocytes that concomitantly express CD45.1 and CD45.2 (F1), whereas recipient mice were congenic only for CD45.2 (**Figure 6**A). Thymus and peripheral lymphoid tissues were analyzed 8 weeks after engraftment of reconstituted TS. In one out of three transplanted mice, the graft could be successfully repopulated (Figure 6B) and harbored thymocytes exclusively of recipient origin (Figure 6C), demonstrating that the hematopoietic cells initially seeded had been completely replaced by host-derived cells since the time of engraftment. The TS supported normal thymocyte development ranging from immature to mature stages of thymocyte development (Figure 6C). Specifically, the most immature $CD24^{pos}$ TCR^{neg} DN cells contained all subsets ranging from early thymic DN1 progenitors to cells with a DN4 phenotype, indicative of successful β-selection (Figure 6C; blue arrow gating).[36] We also analyzed the developmental progression of positively selected CD4 SP cells and detected both

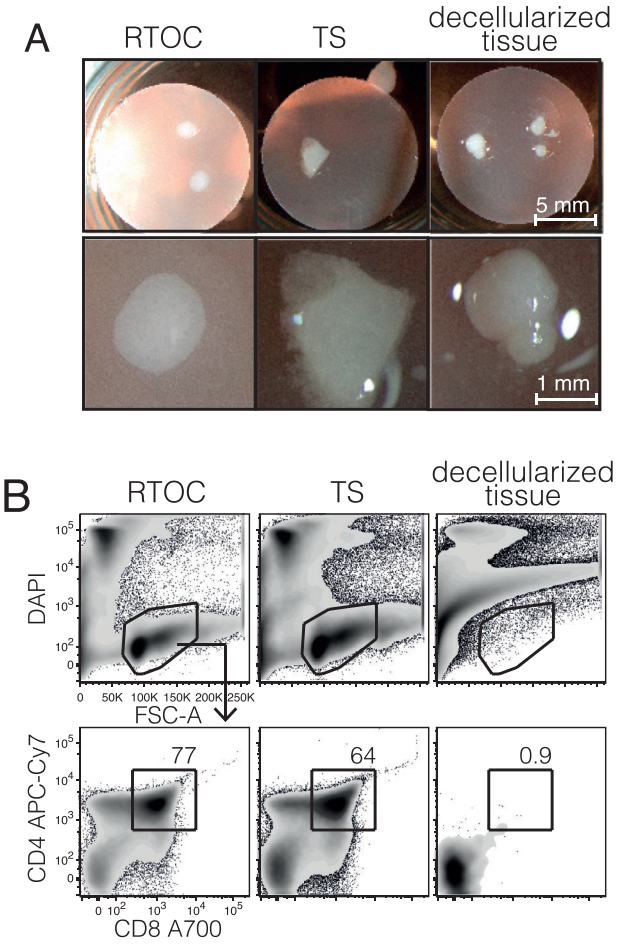

Figure 5. TS seeded with fetal E14.5 stroma cells support the development of E14.5 $CD4^{neg}CD8^{neg}$ DN thymocytes to the $CD4^{pos}CD8^{pos}$ DP stage in vitro. Single-cell suspensions obtained from collagenase digested fetal E14.5 thymic lobes were seeded on TS or mixed with decellularized tissue that has not been subjected to freeze/dry cycles. Reaggregate thymic organ cultures (RTOC) without TS were set up as positive controls. A) Macroscopic appearance of organoids after 5 d culture on floating filters and B) flow cytometric analysis of CD4 and CD8 expression. Data for RTOC and TS are representative of two independent experiments.

early $CD69^{pos}$ $CD24^{pos}$ and late $CD69^{neg}$ $CD24^{low}$ cells in an expected 2:1 ratio (Figure 6C; red arrow gating).[37] Furthermore, regulatory CD4 T cells (characterized by the expression of CD25 and the transcription factor Foxp3) were readily detected (Figure 6C). The architectural organization of the repopulated graphs revealed a normal segregation into an outer, densely populated cortex structured by cytokeratin (ck) 8 expressing TEC and centrally located medullary islands composed of cytokeratin 14-positive TEC and fewer hematopoietic cells (Figure 6D). TS are therefore able to support thymopoiesis for at least 8 weeks.

We then investigated whether T cells generated in the thymus organoid could be exported and populated secondary lymphoid tissues. Lymph nodes of nude mice with a TS graft contained 22% T cells that were predominantly derived from the recipient's bone marrow ($CD45.1^{neg}$, 15.8%, versus 6.8% $CD45.1^{pos}$ originating from the seeded scaffold; Figure 6E). T cells successfully generated in and exported from the graft were subject to lymphopenia-induced proliferation (LIP).[38] This process expands peripheral T cells in response to homeostatic signals such as IL-7 and IL-15, and is characterized by the phenotypic conversion of a naïve ($CD62L^{pos}$/$CD44^{neg}$) to an effector/memory phenotype ($CD62L^{neg}$/$CD44^{pos}$). A higher proportion of $CD45.1^{pos}$ T cells adopted an effector/memory phenotype when compared to host-derived $CD45.1^{neg}$ T cells, as the former had seeded the periphery first (70% vs 8.3% among CD8 T cells, and 78.2% vs 45.6% in CD4 T cells). Moreover, the populations of both donor- and host-derived T cell populations contained an increased frequency of regulatory T cells (Treg; 22.8% and 18.6%, respectively), albeit their frequencies were significantly higher in the grafted, lymphopenic mice when compared to wild type animals (5–10%).[39] In stark contrast, lymph nodes of nongrafted nude mice contained 1% T cells and none of them displayed a naïve or regulatory phenotype (Figure 6E).

Next, we tested the functional competence of donor-derived conventional and regulatory $CD4^+$ T cells generated in TS grafted nude mice. For this purpose, conventional T cells were labeled with CellTrace Violet and mitogenically activated via their T cell receptor in the presence or absence of regulatory T cells (Figure 6F). The robust in vitro proliferative response of conventional T cells (66% ± 2.5%) was significantly reduced in the presence of Treg (25.1 + 1.1%) revealing the functionality of both T cell subpopulations in grafted nude mice (Figure 6G). Treg suppressive function was higher than what is normally seen in wild-type Treg, since lymphopenia leads to an overrepresentation of Treg with an effector phenotype correlating with superior suppressive potential.[40]

2.4. TS Seeded with Adult TEC Can Support T-Cell Development

Adult TEC proliferate less in comparison to embryonic cells[41] and lose their ability to re-aggregate from a single cell suspension into a 3D stromal network, rendering them unsuitable to be investigated in RTOCs.[18] We therefore queried whether adult TEC could form a functional stromal scaffold and maintain their thymopoietic competence when grown in vitro in the context of TS. TEC and DN thymocytes sorted from 4 to 5 week old mice were seeded into TS and monitored for lymphoid differentiation (**Figure 7**A). Thymocytes adopted the TEC-dependent DP phenotype within 5 d, although this differentiation was not efficient since only 7.3% of thymocytes expressed both co-receptors under the chosen conditions (Figure 7B). This low DN to DP conversion rate may, however, be the consequence of how adult TEC were isolated as they needed to be sorted by flow cytometry. Indeed, a similar low conversion rate was observed with sorted fetal TEC (10.5%; Figure 7C) which was in sharp contrast to experiments presented above where the direct seeding of cells obtained from digested fetal thymic lobes achieved a much better efficiency (64%, Figure 5D). Hence, this comparative analysis suggested that the required sorting step impaired TEC function.

To bypass the need for TEC sorting, we changed the experimental design and seeded TS with adult thymic stromal cells from which hematopoietic ($CD45.1^{pos}$) cells had been largely depleted. The repopulated TS were grafted into congenic CD45.2 athymic nude mice ($CD45.2^{pos}$) and analyzed 8 weeks later (**Figure 8**A). Under these conditions, one of five grafts succeeded

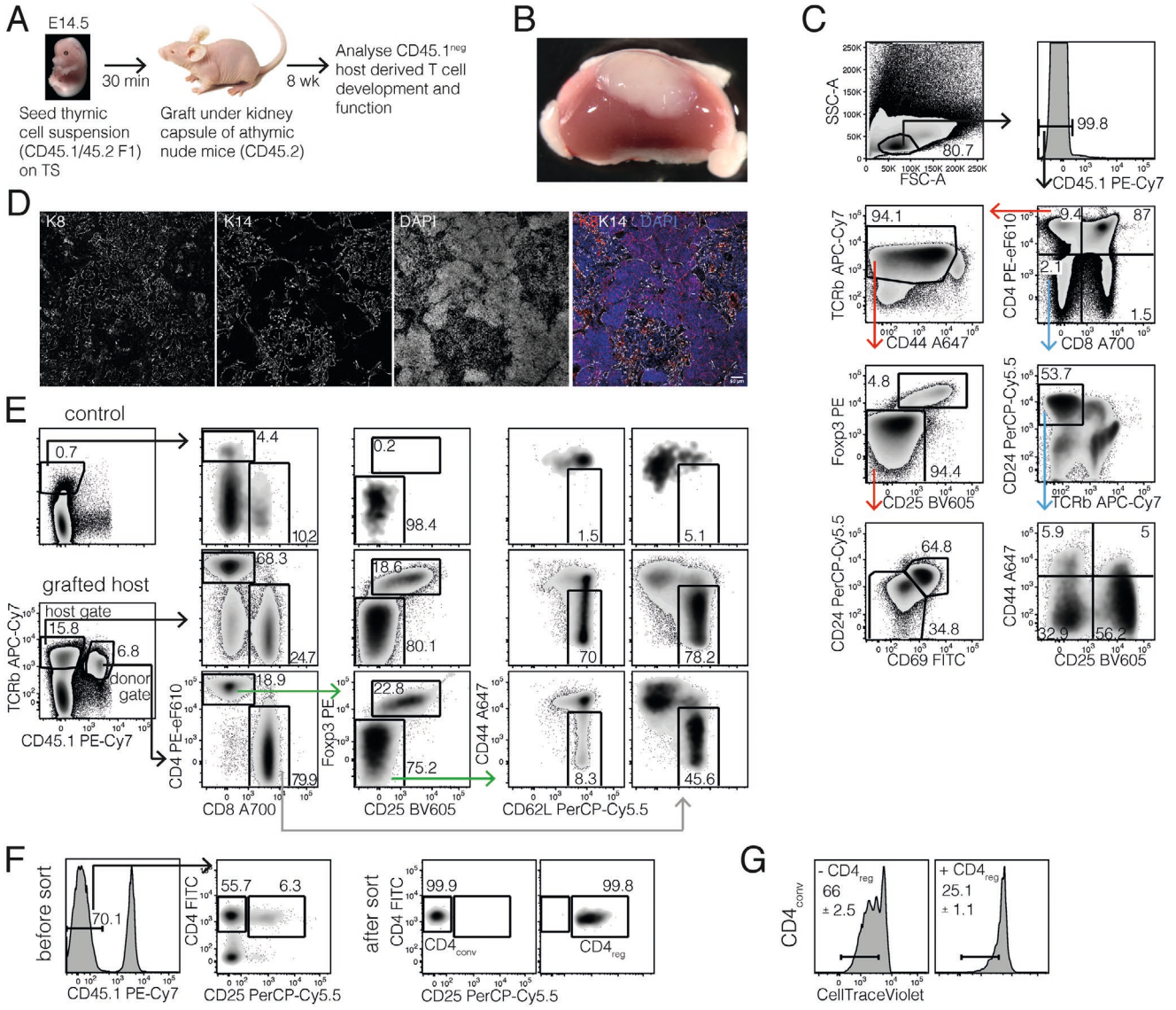

Figure 6. TS seeded with fetal TEC and grafted into athymic recipient mice support continuous de novo development of functionally competent thymocytes that repopulate the peripheral lymphoid organs. A) Schematic setup of in vivo TS grafting using congenic athymic nude mice. B) Kidney of host showing the successful establishment of thymic organoid 8 weeks after transplantation in one of three mice. C) Flow cytometric analysis of host-derived T-cell developmental stages within the graft. Blue arrow gating shows the maturational progression of early thymic progenitors, red arrow gating details CD4 SP differentiation stages. D) Immunohistological analysis of graft section detailing cytokeratin 8 (red) and cytokeratin 14 (gray) expression combined with nuclear DAPI stain (blue). E) Lymph nodes of grafted or control nude mice were stained for donor ($CD45.1^{pos}$) and host ($CD45.1^{neg}$) derived T cells. Naïve CD8 (gray arrow gating) and CD4 T cells (green arrow gating) were quantified and CD4 T cells were additionally analyzed for the presence of regulatory cells. F) Host derived CD4 T cell sort strategy and purities of conventional ($CD4_{conv}$) and regulatory ($CD4_{reg}$) cells. G) In vitro proliferation of CD3 stimulated $CD4_{conv}$ in the absence or presence of $CD4_{reg}$ added in a 1:2 ratio after 3 d of culture. Numbers indicate frequencies of divided cells with standard deviation ($n = 4$ w/o $CD4_{reg}$, $n = 3$ with $CD4_{reg}$).

to be populated by host-derived thymocytes that represented distinct maturational stages (Figure 8B) including immature $CD69^{neg}$ DP cells (83%) and 13% cells that had undergone positive selection (as characterized by an up-regulation of CD69 and TCR and progression to a single CD4 positive stage).[42]

Lymph nodes of grafted athymic mice comprised a small number of T cells, which had originated from both grafted donor cells and endogenous host precursors. Lymph nodes isolated from the host mouse with graft resident DP cells contained equal amounts of both donor and host-derived T cells (Figure 8C, left panels). Peripheral T cells could also be recovered from transplanted athymic mice that did not maintain a graft and thus lacked thymocytes. However, their host-derived T cells bore almost exclusively a CD8 positive phenotype (Figure 8C, middle panels). This feature is characteristically observed in older, athymic mice and reflects the animals' ability to generate $CD8^+$ T cells extrathymically and at low frequency.[43] Lymph nodes of grafted animals also contained donor-derived

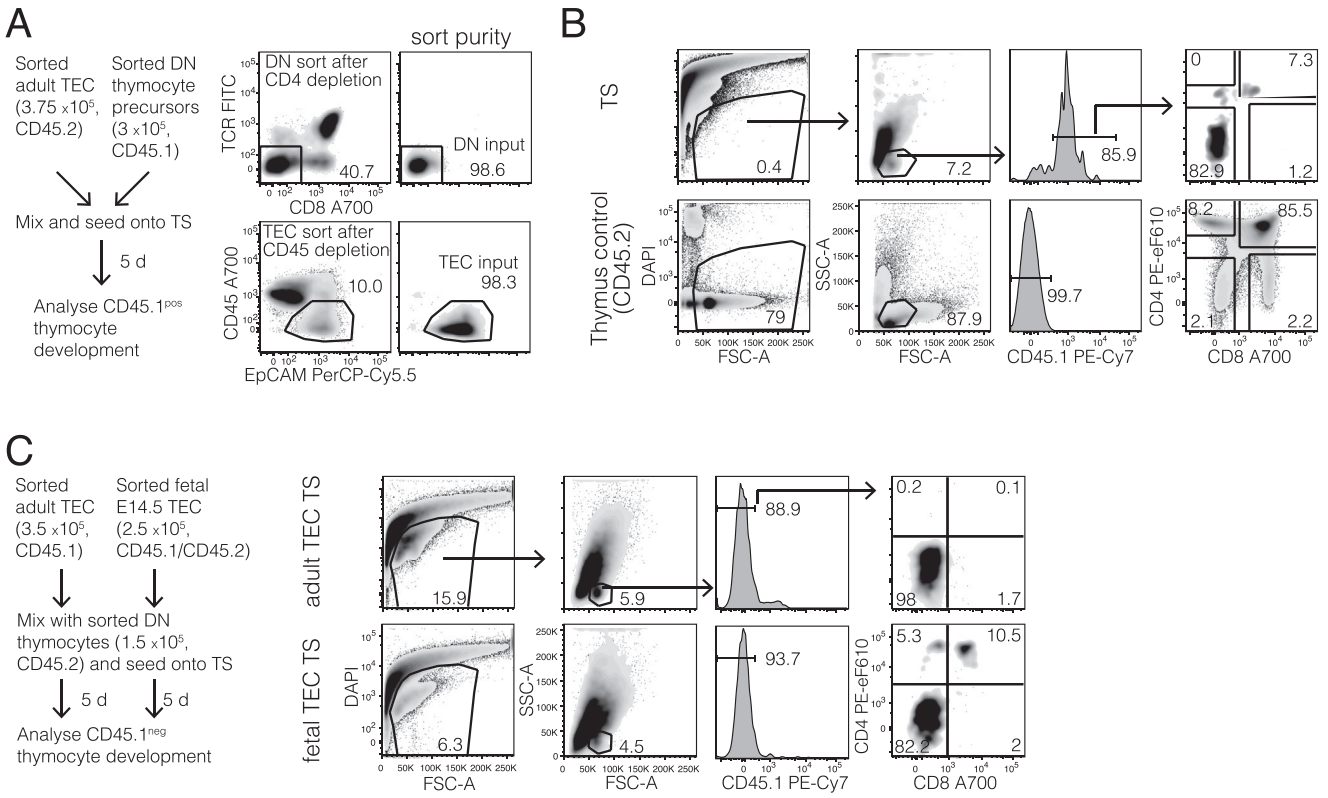

Figure 7. TS seeded with FACS sorted adult or embryonic TEC support limited thymocyte development from the DN to the DP stage in vitro. A) Schematic setup of TS cultures with FACS sorted CD45^{neg}EpCAM^{pos} adult TEC and TCR^{neg} DN thymocytes. Phenotypes before and after sorting are shown. B) Analysis of CD4 and CD8 expression after 5 d of culture in adult TEC seeded TS. Gating strategies and control thymus stain are shown. C) Schematic setup and outcome of TS cultures comparing the developmental progression of sorted DN thymocytes seeded on TS with either FACS sorted adult or fetal TEC.

regulatory T cells at a relatively high frequency reflecting their LIP. Instead, host-derived regulatory T cells were only observed in the grafted mouse where thymocytes could be detected, albeit their frequency was very low (1%; Figure 8C, right panels). Hence, TS populated by adult TEC supported the generation of conventional and regulatory CD4 T cells. Sustained thymopoiesis in TS grafts was observed only occasionally, despite an initial export of donor-derived T cells (Figure 8D,E). Small graft size, low output, and consequent low peripheral cellularity precluded further analyses (e.g., cTEC and mTEC subset composition, TCR repertoire, and T-cell function). While our findings are unprecedented in reporting T cell development with adult TEC in TS for thymic regeneration, we acknowledge the so far uncontrolled reproducibility of the process and the need for further development to improve the robustness of the approach.

2.5. TS Allow for Extended Growth of Adult TEC in Culture

We therefore wished to test whether TS could maintain TEC growth over an extended period of time, a prerequisite critical for sustained thymopoiesis. For this purpose, we monitored by confocal microscopy TS that had been seeded with green fluorescent protein (GFP) expressing, TEC enriched cell suspensions isolated from 4 to 5 week old mice. TEC enriched cell suspensions from wildtype mice plate-cultured in CnT-57 medium for 10 d almost exclusively consisted of EpCAM^{pos} cells (**Figure 9**A), hence ruling out major non-TEC contaminants contributing to the GFP signal. Cell seeding onto TS proved easy and highly efficient, with the whole cell suspension promptly absorbed into the 3D scaffolds. Neither floating cells in the culture medium, nor cells adherent to the culture plates were detected during culture. Confocal imaging 2 hours after seeding showed uniform distribution of cells throughout the scaffold (Figure 9B). Following an initial phase marked by the disappearance of the majority of the labeled cells, TEC cellularity progressively recovered—with GFP positive areas growing over time, particularly along the edges of the constructs (Figure 9B). Positivity for K8 identified cortical TEC, while K14 indicated the presence of medullary TEC, many cells coexpressing K8 and K14 (**Figure 10**, top row). Organoids were finally also analyzed for the expression of Foxn1, a transcription factor essential for TEC growth, differentiation, and function.[16] Using immunofluorescence on sections of organoids, nuclear Foxn1 stains were detected in cells as late as 30 d after their seeding into TS (Figure 10, bottom row). These findings suggest that TS support the maintenance of adult TEC in vitro over an extended period of time.

3. Discussion

In this study, we developed a 3D scaffold based on extracellular matrix from decellularized thymic tissue, designated TS.

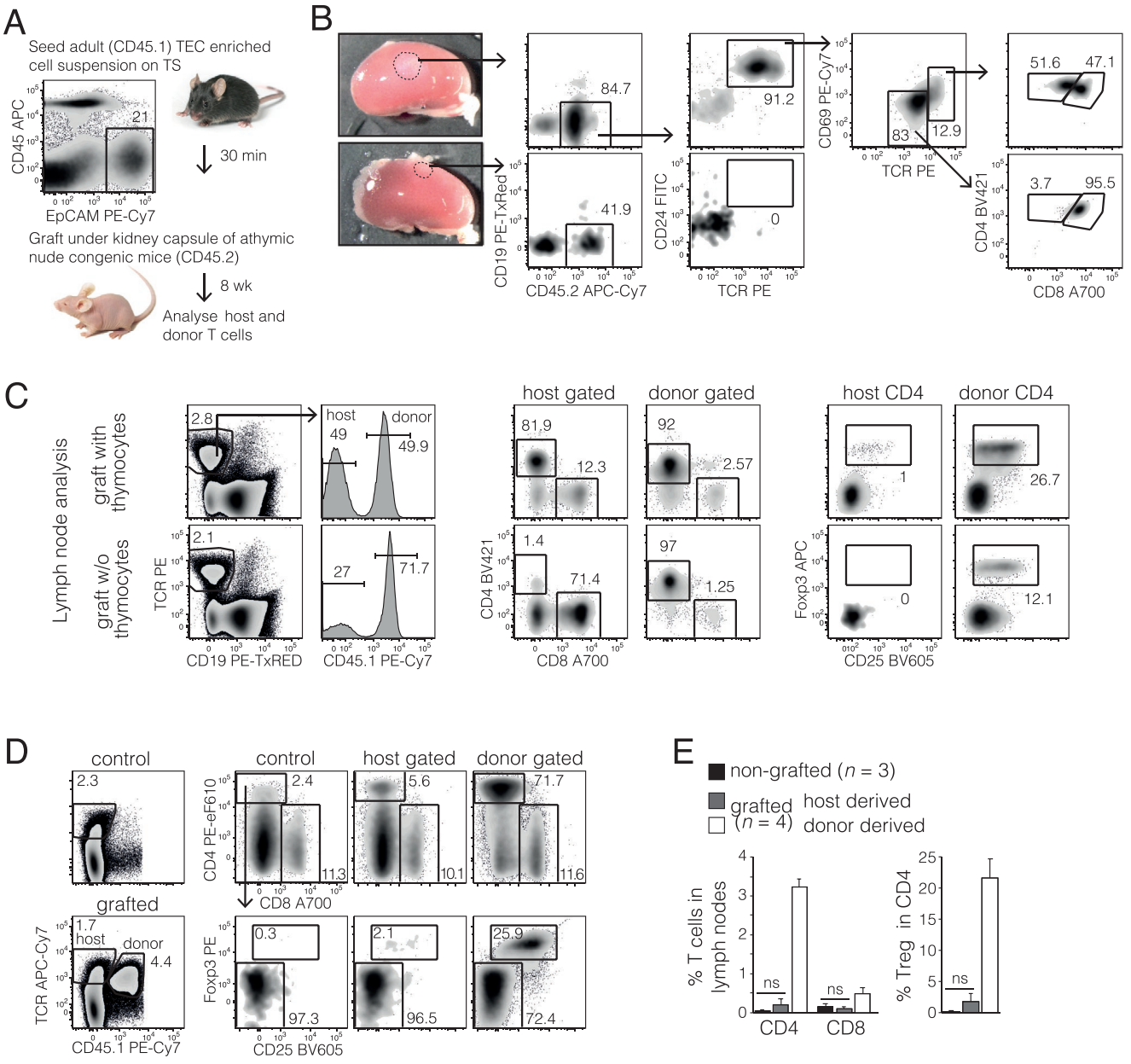

Figure 8. TS seeded with adult TEC enriched cell suspensions and grafted into athymic recipient mice support de novo development and export of host-derived T cells. A) Schematic in vivo setup of TS seeded with TEC enriched cell suspension isolated from CD45.1 adult mice thymic and grafted into CD45.2 congenic athymic nude mice. Phenotype of CD45 depleted, TEC enriched cell suspension is displayed. B) Kidneys of host mice showing graft remnants (outlined) and their thymocyte phenotype. C) T cell composition within the lymph nodes of the hosts harboring grafts with or without resident thymocytes as shown in B. D) Representative flow cytometric and E) quantitative analysis of host and donor derived T cell subsets 8 weeks after grafting TEC enriched adult thymus digests seeded on TS compared to non-grafted control animals. Data represent two independent experiments with B) 1 out of 2 and D,E) 0 out of 4 successful reconstitutions.

When seeded with either fetal or adult TEC, TS could support with different efficiency the maturation of lymphoid precursors to conventional and regulatory T cells able to respond to mitogenic stimuli.

The successful engineering of a functional thymic microenvironment critically depends on the ex vivo growth of adult TEC. The preservation of the cells' thymopoietic capacity has, however, been one of the major shortcomings in creating in vitro a thymus organoid.[18] This inability constitutes thus a critical difficulty that needs to be effectively solved to establish, investigate and manipulate T cell development, be it to develop an in vitro platform for experimental studies or an organ for in vivo replacement efforts. Despite the lack of optimization in structural and cellular conditions, possibly reflected in the rather limited outcome robustness, our results provide the first description of engineered conditions that allow adult TEC to survive over an extended period of time both in vitro and in vivo whilst supporting thymopoiesis.

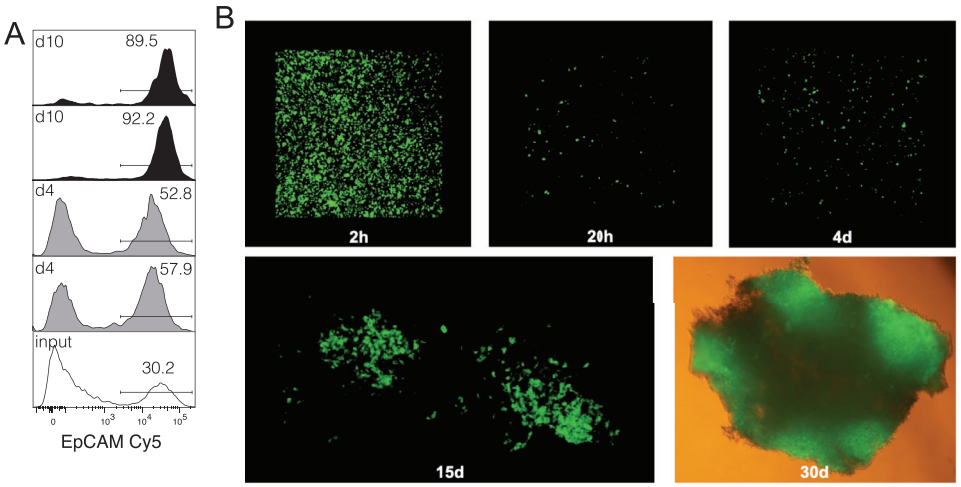

Figure 9. TS support long-term in vitro maintenance of adult TEC. A) Frequencies of EpCAM^{pos} cells derived from TEC enriched cell suspensions after 4 and 10 d of culture in CnT-57 medium. B) Confocal images of TEC enriched GFP+ cells cultured in vitro onto 3D thymus scaffolds at different time-points after seeding.

The ability to engineer a microenvironment supporting thymic function was based on combining and refining protocols to decellularize murine thymus tissue. For this objective, we employed perfusion bioreactors to ensure efficient distribution of reagents throughout the sample volume while also allowing for an enhanced removal of cell debris by extensive washes. With the samples stably positioned in the bioreactor, tissue stress was controlled to a minimum thus preserving key proteins of the native ECM,[44] which have been previously shown to play a crucial role in determining TEC morphology, functionality, and the interactions with developing T cells.[45,46] In future, a more extensive matrisome analysis at distinct developmental stages might reveal additional relevant elements in the compositional identity of the scaffolds, which should be controlled for the fabrication of improved substrate materials for thymus engineering purposes. Tunable microenvironments in combination with proper immune cell types or organoids will provide unprecedented opportunities to investigate organ physiology and immune response ex vivo, and to test and implement novel therapeutic strategies.[47,48]

Several shortcomings had been encountered with decellularized thymus used in the past to generate organoids that support fetal and neonatal TEC growth.[25,26] For example, the decellularized whole organ is difficult to handle and cell seeding is particularly challenging, resulting in limited cell penetration and unequal cell distribution. In addition, the acellular whole organ cannot be controlled in size and shape. To overcome these and other limitations related to the use of a native tissue

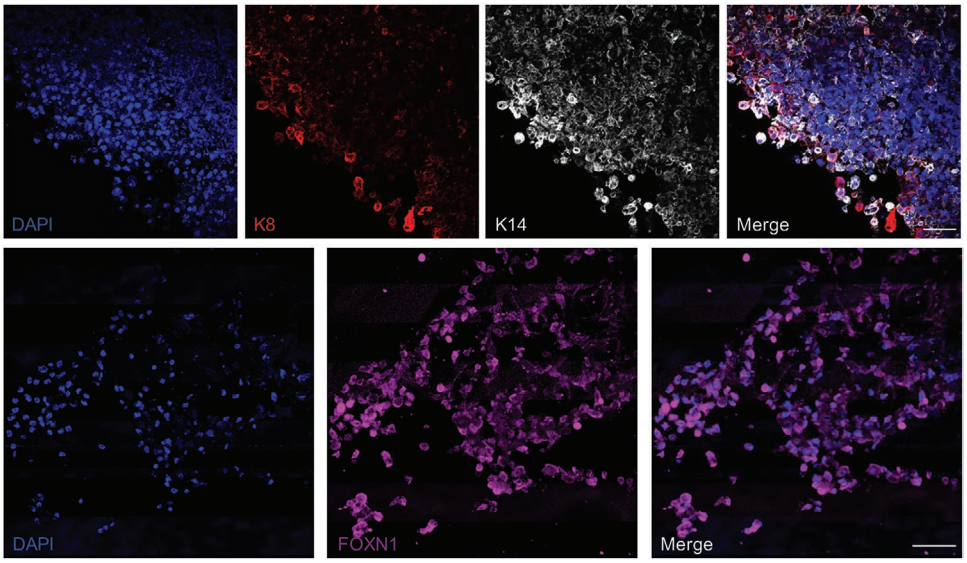

Figure 10. TS support prolonged in vitro culture of adult TEC expressing characteristic markers. Immunofluorescence analysis for the expression of cytokeratin 8 (K8, cortical TEC marker, red) and cytokeratin 14 (K14, medullary TEC marker, white), and of FoxN1 (transcription factor, pink) by adult TEC after 30 d of in vitro culture onto TS. Nuclei were stained by DAPI (blue). Scale bars: 50 µm.

acellular framework, we generated a porous 3D scaffold from decellularized thymic tissue. The resultant structure provided a uniform pattern of interconnected pores with improved water uptake capacity, favoring not only efficient cell seeding and expansion but also mass transfer throughout the scaffold volume.

While robust for manipulations in vitro over an extended period of time, TS could not be detected in most of recipient mice 8 weeks after grafting. The resorption of these tissues under in vivo conditions prevented sustained thymopoiesis, as previously observed with an analogous approach.[24] A future task will therefore be to tune the physical properties of the scaffold to change the degradation kinetics of the TS whilst still ensuring efficient in situ growth and preservation of functional TEC. Moreover, the approach chosen will allow to render the size and shape of the scaffold bespoke to individual needs, as well as to optimize the microstructure of the scaffold to better mimic the native tissue microenvironment. Overall, the processing of decellularized thymus into a 3D porous scaffold represents an important conceptual and practical advance, allowing to regulate "by design" the properties of the generated materials.

To our knowledge, our study offers the first report on the nanomechanical properties of thymus tissue. Future work will be required to investigate which mechanical cues are critical in supporting TEC maintenance and function, and to optimize the scaffold production process accordingly. Interestingly, as compared to all other analyses, the results of nanomechanical testing on the 3D scaffolds showed the highest variability, possibly implying that variability in nanomechanical properties is one key factor associated with the reported limited robustness of biological results. In this perspective, atomic force microscopy analyses could be envisioned as quality control of production batches, to ensure adequate quality of the starting material and process standardization. Increased control and reproducibility of the scaffold properties will be crucial for the development of a reliable model for investigating TEC biology in vitro and for translational applications of thymus engineering strategies.

In addition to improving the engineering of TS, efforts will also need to be directed at identifying TEC precursors with a long-term repopulation potential able to give rise to all TEC lineages and subpopulations. The use of single-cell transcriptomic data derived from mouse TEC has revealed a considerable complexity of TEC subtypes[18,49,50] and informed computational efforts to define the developmental trajectory of these cells. Long-term repopulating TEC precursors seeded onto appropriate TS will secure the maintenance of an environment competent to attract blood borne T-cell precursor and direct over an extended period of time their differentiation and selection to mature conventional and regulatory T cells. Improved protocols for cell retrieval after in vitro culture will be required for in-depth phenotypic and quantitative investigations of TEC. As these TEC precursors are most likely fragile, conditions will need to be deployed that guarantee an efficient, swift, and uniform seeding onto the ECM scaffold and that also allow to supplement these basic environments with additional stromal cells including mesenchymal and endothelial cells, known to contribute to thymic cross-talk. Using perfusion bioreactors[51] and selective conditions will further assist in creating ex vivo a self-organizing thymic microenvironment that provides robust sustained T cell output. The precise control of the chemo-physical conditions that regulate in vitro thymus tissue formation are critical for reproducibility and scaling, be it to generate smaller organoids for drug screening or larger microenvironments for organ replacement strategies as a therapeutic option for individuals without or with a hypoplastic thymus.

4. Experimental Section

Mice: Athymic C57BL/6 nu/nu (nude) mice were purchased from Taconic, C57BL/6 mice were obtained from Janvier, C57BL/6 CD45.1, C57BL/6-Tg(CAG-EGFP)1Osb/J (TgN) and C57BL/6 Rag2$^{-/-}$ mice were bred and maintained at the University of Basel Department of Biomedicine's SPF facility. Unless otherwise noted, donor mice for scaffold preparations were 4 to 6 weeks of age and host mice for transplants were 6 and 10 weeks of age. For developmental staging, the day of the vaginal plug was designated as E0.5. All animals were kept under specific pathogen-free conditions and experiments were carried out in accordance with local and national regulations and permissions.

Thymus Decellularization: Different decellularization protocols using trypsin and Triton X-100, peracetic acid, or sodium deoxycholate were screened in preliminary experiments. As compared to all other protocols tested, the use of milliQ water and DNase as detailed below achieved the best results in terms of cell removal and preservation of the native thymus ECM (data not shown). Thymic lobes were separated and cleaned from all overlaying loose connective and adipose tissues and rinsed 4 times (30 min each) in PBS. Thereafter, the thymi were subjected to the following steps for decellularization: tissue was washed in milliQ water supplemented with 2% antibiotic/antimycotic solution (Sigma) for 72 h at 4 °C, with solution changed every 12 h, then treated with DNase-I (2000 kU) in 1 mol L^{-1} NaCl (Sigma) for 2 h at RT and finally rinsed with PBS for 72 h at 4 °C. The whole decellularization process was performed under perfusion flow in a bioreactor system[52] (currently distributed as U-CUP by Cellec Biotek AG) at a flow rate of 0.3 mL min^{-1}, for improved efficacy (data not shown). Two thymic lobes were placed in the perfusion chamber of each bioreactor, supported by two EFTE nylon meshes (Fluorotex Sefar) and a custom-made PTFE spacer to ensure stable positioning of the sample and favor perfusion through the tissue. Easy and safe exchange of the solutions was performed via a set of valves on both sides of the perfusion chamber.

3D Scaffold Preparation: Decellularized thymi were homogenized at 4 °C and poured into 96-well plates. The samples were frozen at −20 °C for 18 h, transferred to a −80 °C freezer for another 18 h and lyophilized overnight to generate 3D porous scaffolds. For improved stability and handling, crosslinking of the thymus scaffolds (TS) was performed by immersion in absolute ethanol overnight at 4 °C and chemical crosslinking in a *N*-(3-dimethylaminopropyl)-*N*′-ethylcarbodiimide hydrochloride (EDC, Sigma-Aldrich) and *N*-hydroxysuccinimide (NHS, Sigma-Aldrich) solution in ethanol 95% at 4 °C for 6 h. Scaffolds were then washed in 0.1 M disodium hydrogen phosphate (Na_2HPO_4, Merck) for 2 h followed by four rinsing steps of 30 min in double-distilled water and additional three steps of 24 h in PBS (Invitrogen). Scaffolds were rinsed overnight with 70% ethanol, properly washed in sterile PBS, and stored in sterile PBS at 4°C until use.

Histology and DNA Quantification: Native and decellularized thymi were fixed overnight with 4% paraformaldehyde at 4 °C, then rinsed in PBS and embedded in paraffin. Sections 5 µm in thickness were stained with hematoxilin & eosin staining to visualize nuclear content and tissue microstructure.

To assess the efficiency of the decellularization method, the total DNA content was quantified in native and treated thymi. Thymus lobes were weighted and then homogenized by Mikro-Dismembrator S (Sartorius).

The total DNA was extracted by DNeasy Blood & Tissue Kit (Quiagen) and quantified by Quant-iT PicoGreen dsDNA Assay kit (Quiagen) according to the manufacturer's instructions. Data are presented as mean and standard deviation of $n = 6$ samples per group.

Immunofluorescence for ECM Proteins: Native thymi, decellularized tissues, and 3D scaffolds were fixed with 4% paraformaldehyde overnight at 4 °C, embedded in OCT (Tissue-Tek) and cross-sectioned (10 µm thick). Sections were rinsed with PBS and blocked with PBS/2% BSA. Tissues were then incubated overnight with monoclonal anti-Collagen IV (ab6586, Abcam), Laminin (ab128053, Abcam) or fibronectin (ab2413, Abcam) primary antibodies. After rinsing in PBS, samples were incubated for 40 min at RT with Alexa Fluor 488, 546, or 647 secondary antibodies (Abcam). After rinsing in PBS, nuclei were stained with DAPI. Imaging was performed with a confocal microscope (Zeiss LSM 710).

Scanning Electron Microscopy (SEM): For SEM, samples were fixed for 2 days in 0.1 M cacodylate-buffered 2% glutaraldehyde at pH 7.2 at 25 °C. After dehydration in graded ethanol series solutions (30, 50, 75, and 100% EtOH concentration) and critical point drying, samples were sputter-coated with gold before examination with a Philips XL 30 ESEM microscope. The microstructure of the 3D thymus scaffolds was assessed qualitatively on longitudinal and transversal sections.

Protein Quantification: Protein content was quantified in native thymi and 3D thymus scaffolds by BCA and ELISA assays. Samples were frozen at –80°, mechanically disrupted in liquid nitrogen, and dissolved in radioimmunoprecipitation assay buffer (RIPA buffer, Sigma-Aldrich) modified with phosphatase and protease inhibitors (Roche) used according to the manufacturer's instructions. The total amount of proteins was assessed by BCA protein assay (Thermo Fisher Scientific) on properly diluted samples. Samples were then further diluted and assessed for laminin (#119572, Abcam), fibronectin (#210967, Abcam) and collagen IV (NBP2-75862, Novus Biologicals). Each assay was performed according to manufacturer instructions.

Swelling Behavior and Water Content: The swelling behavior of native thymus, decellularized tissue, and 3D scaffolds was investigated by immersion in PBS at 37 °C up to 24 h. At defined time-points (30 min, 3 h, 18 h, and 24 h), the samples were collected from PBS, excess liquid was removed with filter paper and the wet weight was recorded (Ww). The swelling ratio was calculated using the following formula:

$$\text{Swelling ratio}(\%) = \left[(W\text{w} - W\text{d})/W\text{d}\right] \times 100 \quad (1)$$

where W_d is the initial weight of the lyophilized sample. The weight of wet samples was evaluated three times for each sample, to account for methodological errors induced by the blotting step.

Water content (%) of native thymus, decellularized tissue, and 3D scaffolds were estimated by ponderal evaluation of the weight of the wet samples at equilibrium, blotted with tissue paper, and the weight of the lyophilized samples according to the following equation:

$$\text{Water content}(\%) = \left[(W\text{w} - W\text{d})/W\text{w}\right] \times 100 \quad (2)$$

where W_d = weight of the lyophilized samples, W_w = weight of the wet samples after 24 h of immersion in PBS at 37 °C. Data are presented as mean and standard deviations ($n = 4$ native thymic lobes, $n = 3$ decellularized lobes, and $n = 4$ scaffolds).

Nanomechanical Characterization: Nanomechanical characterization by atomic force microscopy (AFM) was performed using the ARTIDIS research device (ARTIDIS AG, Basel, Switzerland) (Figure 4A). Portions of native thymus (N) ($n = 6$), decellularized tissue (D) ($n = 6$), and thymus scaffolds (TS) ($n = 7$) were placed in standard TPP 9.2 cm^2 dishes (TPP, Switzerland) pretreated with poly-L-lysine (Sigma Aldrich, USA). Samples were firmly attached to the substrate by centrifugation at 3500 rpm for 10 min and stored in PBS at 4 °C until further use.[53] For each group (TS, N, D), at least six samples were prepared for measurements. ARTIDIS chip holder consumables premounted with triangular DNP-S10 D probes (Bruker AFM Probes, USA) with a nominal spring constant of 0.06 N m^{-1}, cantilever length of 205 µm, tip height of 7 µm, and tip radius of 20 nm were used for the measurements. Fully automated calibration including spring constant determination in the air using the thermal tune method as described by Sader and co-workers was performed.[54] Deflection sensitivity calibration was performed by acquiring force curves at the bottom of TPP-9,2 cm^2 dishes filled with degassed, sterile PBS solution.[32] Optical microscopes (Leica, Germany and Navitar, USA) integrated into the ARTIDIS device allowed imaging and positioning control of cantilever and sample. For determining the elastic modulus of the sample, the AFM was operated in a force–volume mode, whereby 20 × 20 force–displacement curves were recorded in square arrays (i.e., force maps) each covering an area of 20 × 20 µm^2, generating 400 force curves per map. For each sample, force maps were acquired on at least 20 equidistant spots across the sample. All force–displacement curves were sampled with indentations ranging between 0.2 and 3 µm at a defined maximum force load[29,32] of 1.8 nN at an indentation velocity of 16 µm s^{-1}. AFM data were analyzed using the ARTIDIS analysis software. Briefly, the acquired curves were tilted, corrected, and transformed to generate force versus tip–sample distance curves. The backward elastic modulus was calculated and used for analysis.[55] Signal-to-noise ratio, baseline tilt, and curve twist were used to filter suitable maps for analysis.[56] Samples containing less than five maps with good force curves were discarded. The average of the median per force map was considered as the representative modulus for a sample. Boxplots were created from the average sample modulus. Cumulative histograms were created directly from the backward elastic modulus of all force curves of a sample. The frequency is normalized to range from 0 to 1. Force maps were further processed using Gwyddion for visualization.[57]

Cell Isolation: For fetal TEC isolation, E14.5 thymic lobes were digested with Collagenase D and DNaseI (Roche Diagnostics; 1 mg mL^{-1} and 30 µg mL^{-1}, respectively; 15 min, 37 °C) and single-cell suspensions were obtained by pipetting up and down. For adult TEC isolation, thymic lobes were cleaned from fatty tissues and incubated with Liberase and DNaseI (Roche Diagnostics; 200 µg mL^{-1} and 30 µg mL^{-1}, respectively; 45 min, 37 °C). Single-cell suspensions were obtained by sequential pipetting steps using progressively decreasing tip openings. Cell suspensions were subsequently filtered through a nylon mesh (100 µm pore size, Sefar Nitex) to remove debris. Adult TEC were magnetically enriched by using mouse CD45 microbeads and the AutoMACS Pro Separator (Miltenyi Biotec). Whole thymus and lymph node cell suspensions were prepared by gently squeezing organs between two nylon meshes (100 µm pore size, Sefar Nitex) in PBS containing 2% heat-inactivated FCS (FACS buffer). Prior to thymocyte sorting, cell suspensions were magnetically depleted of CD4 cells using biotinylated CD4 mAb, anti-Biotin microbeads (Miltenyi Biotec) and the AutoMACS Pro Separator.

Flow Cytometry: Fluorophore labelled mAb CD4 (GK1.5), CD8a (53-6.7), CD25 (PC 61), CD44 (IM7), CD45 (30-F11), CD45.1 (A20), CD45.2 (104), CD62L (MEL-14), CD69 (H1.2F3), EpCAM (G8.8), and TCR (H57-597) were obtained from BioLegend, Foxp3 mAb (FJK-16s, eBioscience), PE-eF610 conjugated CD4 (GK1.5, eBioscience) and PE-TxRed conjugated CD19 (6D5, Life Technologies) were purchased from ThermoFisher Scientific. Cells were incubated for 30 min on ice with mAb cocktails, washed in FACS buffer (PBS/2% FCS), and acquired/sorted on BD FACSFortessa and BD FACSAriaII cytometers (Becton Dickinson). Analyses were performed using FlowJo software (Becton Dickinson).

TS Assays: TS were cut into quarters and presoaked for 1 h in cell culture medium (IMDM containing 10% FCS, 0.5 × 10^{-3} M 2-ME, 100 µg mL^{-1} kanamycin, Life Technologies) and let to dry. RTOC and decellularized thymus tissue were seeded with cell slurries containing approximately 5 × 10^5 cells (E14.5) or 2–4 × 10^6 cells (TEC enriched adult thymus preparations). Bigger in size, TS were seeded with twice the amount of cells. All constructs were then cultured at the liquid/air interface on floating filters with a 0.8 µm pore size (Nucleopore) for the indicated time. Alternatively, after a 30 min interval to let the seeded cells settle inside the TS, the constructs were grafted under the kidney capsule of nude mice. After 6–8 weeks, grafts and lymph nodes (axillary, brachial, inguinal, mesenteric) of host mice were analyzed.

In Vitro T-Cell Proliferation Assay: Sorted CD45.1^{neg}CD25^{neg}CD4^{pos} conventional T cells were labeled with the CellTrace Violet cell proliferation kit (ThermoFisher Scientific) according to the

manufacturer's instructions. 50 000 CD4 T cells were cultured with equal amounts of irradiated (3000 cGy) Rag2$^{-/-}$ splenic accessory cells and 0.5 µg mL^{-1} of CD3 mAb (145-2c11, BioLegend) in the presence or absence of 25 000 sorted CD45.1^{neg}CD25^{pos}CD4^{pos} regulatory T cells. The proliferative response of conventional CD4 T cells was evaluated after 72 h by flow cytometry and assessed by the serial dilution of the CellTrace Violet on labeled CD4^{pos} cells.

3D In Vitro Culture of Adult TEC: TS were cut into quarters and pre-soaked for 1 h in cell culture medium (IMDM containing 10% FCS, 0.5×10^{-3} M 2-ME, 100 µg mL^{-1} kanamycin, Life Technologies) and let to dry. Scaffolds were seeded with 2–4 $\times$ 10^6 TEC enriched GFP$^+$ cells. TS were then cultured at the liquid/air interface on floating filters with a 0.8 µm pore size (Nucleopore) in CnT-57 medium (CELLnTEC) supplemented with ROCK inhibitor (10×10^{-9} M; Calbiochem, Merck) and kanamycin up to 30 d. Medium was replaced every other day. Cell proliferation was monitored over time by confocal microscopy, while TEC phenotype (K8 and K14) and functionality (FoxN1 and Aire) were assessed at day 14, 24, and 30.

Immunofluorescence of In Vitro Cultured Adult TEC: 3D cell constructs at 15, 24, and 30 d after seeding were embedded in OCT (Tissue-Tek) and cross-sectioned (10 µm thick). Frozen sections were fixed with 4% paraformaldehyde for 10 min, stained using antibodies specific for K14 (1:500, Covance), K8 (1:200, TROMA-1, NICHD supported Hybridoma Bank), and FoxN1 (1:1000, provided by T. Amagai, Meiji University of Integrative Medicine, Hiyoshi-cho, Nantan, Japan). Briefly, fixed sections were rehydrated in PBS for 30 min then incubated in a solution of 5% goat serum and 0.5% Tween-20 (Sigma) in PBS for 20 min to block nonspecific bindings and permeabilize cells. Primary staining was performed at RT for 1 h followed by secondary staining for 45 min. Slides were, then, stained with DAPI, and mounted in fluorescent mounting media (Dako, USA). Images were acquired using a Zeiss LSM710 (Carl Zeiss).

Statistical Analysis: All calculations data were performed using GraphPad Prism v2.2 software. Normality was checked with the Shapiro-Wilk test. Statistical significance for comparing two means was calculated using unpaired *t*-tests. To test multiple comparisons, ANOVA and post-hoc Tukey HSD testing were performed. Statistical significance is defined as $p < 0.05$ (*).

Acknowledgements

M.A.A., T.B., G.A.H., and I.M. contributed equally to this work. The authors thank Dr Saulius Žuklys for their assistance with immunofluorescence analyses. Thanks to Sasan Jalili-Firoozinezhad for his input on crosslinking protocols, and to Dr. Manuele G. Muraro and Dr. Alessandro Pirosa for their help with sample preparation during Covid-19 pandemic. Thanks to Boris Dasen and Dr. Morgane Hilpert for their advice on protein quantification analysis. Thanks also to Dr. Laura Power for her tips on statistical analysis. This work was supported by grants from the Swiss National Foundation (3100-68310.02, 3100-122558 and 310030_184672 to G.A.H.). All animals were kept under specific pathogen-free conditions and experiments were carried out in accordance with local and national regulations, and permission of the cantonal veterinary office of Basel-Stadt (2321 issued to G.A.H.).

Conflict of Interest

Philipp Oertle is a shareholder in ARTIDIS AG. Gitika Srivastava and Philipp Oertle are employed by ARTIDIS AG. The other authors declare no conflict of interest.

Data Availability Statement

Supporting information is available from the author upon reasonable request.

Keywords

3D scaffolds, decellularization, thymic epithelial cells, thymus engineering

Received: December 14, 2020
Revised: January 28, 2021
Published online: March 12, 2021

[1] J. F. A. P. Miller, *Nat. Rev. Immunol.* **2011**, *11*, 489.
[2] J. Abramson, G. Anderson, *Annu. Rev. Immunol.* **2017**, *35*, 85.
[3] N. Kadouri, S. Nevo, Y. Goldfarb, J. Abramson, *Nat. Rev. Immunol.* **2019**, *20*, 239.
[4] Y. Takahama, I. Ohigashi, S. Baik, G. Anderson, *Nat. Rev. Immunol.* **2017**, *17*, 295.
[5] D. Ray, R. Yung, *Clin. Immunol.* **2018**, *196*, 59.
[6] G. Pawelec, A. Larbi, E. Derhovanessian, *J. Comp. Pathol.* **2010**, *142*, S39.
[7] A. N. Akbar, S. M. Henson, A. Lanna, *Trends Immunol.* **2016**, *37*, 866.
[8] B. Adkins, D. Gandour, S. Strober, I. Weissman, *J. Immunol.* **1988**, *140*, 3373.
[9] B. Chung, L. Barbara-Burnham, L. Barsky, K. Weinberg, *Blood* **2001**, *98*, 1601.
[10] K. M. Williams, F. T. Hakim, R. E. Gress, *Semin. Immunol.* **2007**, *19*, 318.
[11] W. Krenger, G. A. Holländer, *Semin. Immunopathol.* **2008**, *30*, 439.
[12] A. Tajima, I. Pradhan, M. Trucco, Y. Fan, *Curr. Stem Cell Rep.* **2016**, *2*, 128.
[13] K. L. Anderson, N. C. Moore, D. E. J. McLoughlin, E. J. Jenkinson, J. J. T. Owen, *Dev. Comp. Immunol.* **1998**, *22*, 367.
[14] V. Kont, M. Laan, K. Kisand, A. Merits, H. S. Scott, P. Peterson, *Mol. Immunol.* **2008**, *45*, 25.
[15] M. Mohtashami, J. C. Zúñiga-Pflücker, *J. Immunol.* **2006**, *176*, 730.
[16] S. Žuklys, A. Handel, S. Zhanybekova, F. Govani, M. Keller, S. Maio, C. E. Mayer, H. Y. Teh, K. Hafen, G. Gallone, T. Barthlott, C. P. Ponting, G. A. Holländer, *Nat. Immunol.* **2016**, *17*, 1206.
[17] K. J. Hare, E. J. Jenkinson, G. Anderson, *Semin. Immunol.* **1999**, *11*, 3.
[18] K. Wong, N. L. Lister, M. Barsanti, J. M. C. Lim, M. V. Hammett, D. M. Khong, C. Siatskas, D. H. Gray, R. L. Boyd, A. P. Chidgey, *Cell Rep.* **2014**, *8*, 1198.
[19] E. A. Gosselin, H. B. Eppler, J. S. Bromberg, C. M. Jewell, *Nat. Mater.* **2018**, *17*, 484.
[20] S. Kim, S. B. Shah, P. L. Graney, A. Singh, *Nat. Rev. Mater.* **2019**, *4*, 355.
[21] M. C. Poznansky, R. H. Evans, R. B. Foxall, I. T. Olszak, A. H. Piascik, K. E. Hartman, C. Brander, T. H. Meyer, M. J. Pykett, K. T. Chabner, S. A. Kalams, M. Rosenzweig, D. T. Scadden, *Nat. Biotechnol.* **2000**, *18*, 729.
[22] S. Pinto, K. Schmidt, S. Egle, H. J. Stark, P. Boukamp, B. Kyewski, *J. Immunol.* **2013**, *190*, 1085.
[23] A. Tajima, W. Liu, I. Pradhan, S. Bertera, C. Bagia, M. Trucco, W. S. Meng, Y. Fan, *Clin. Immunol.* **2015**, *160*, 82.
[24] I. Bortolomai, M. Sandri, E. Draghici, E. Fontana, E. Campodoni, G. E. Marcovecchio, F. Ferrua, L. Perani, A. Spinelli, T. Canu, M. Catucci, T. Di Tomaso, L. Sergi Sergi, A. Esposito, E. Lombardo, L. Naldini, A. Tampieri, G. A. Holländer, A. Villa, M. Bosticardo, *Stem Cells Transl. Med.* **2019**, *8*, 1107.
[25] M. Hun, M. Barsanti, K. Wong, J. Ramshaw, J. Werkmeister, A. P. Chidgey, *Biomaterials* **2017**, *118*, 1.
[26] Y. Fan, A. Tajima, S. K. Goh, X. Geng, G. Gualtierotti, M. Grupillo, A. Coppola, S. Bertera, W. A. Rudert, I. Banerjee, R. Bottino, M. Trucco, *Mol. Ther.* **2015**, *23*, 1262.

[27] P. M. Crapo, T. W. Gilbert, S. F. Badylak, *Biomaterials* **2011**, *32*, 3233.
[28] E. Melo, P. Oertle, C. Trepp, H. Meistermann, T. Burgoyne, L. Sborgi, A. C. Cabrera, C. Y. Chen, J. C. Hoflack, T. Kam-Thong, R. Schmucki, L. Badi, N. Flint, Z. E. Ghiani, F. Delobel, C. Stucki, G. Gromo, A. Einhaus, B. Hornsperger, S. Golling, J. Siebourg-Polster, F. Gerber, B. Bohrmann, C. Futter, T. Dunkley, S. Hiller, O. Schilling, V. Enzmann, S. Fauser, M. Plodinec, R. Iacone, *EBioMedicine* **2018**, *27*, 258.
[29] A. Glentis, P. Oertle, P. Mariani, A. Chikina, F. El Marjou, Y. Attieh, F. Zaccarini, M. Lae, D. Loew, F. Dingli, P. Sirven, M. Schoumacher, B. G. Gurchenkov, M. Prodinec, D. M. Vignjevic, *Nat. Commun.* **2017**, *8*, 924.
[30] M. Reyes-Lua, P. Oertle, L. Camenzind, A. Goz, C. H. Meyer, K. Konieczka, M. Loparic, W. Halfter, P. B. Henrich, *Invest. Ophthalmol. Visual Sci.* **2016**, *57*, 2839.
[31] M. To, A. Goz, L. Camenzind, P. Oertle, J. Candiello, M. Sullivan, P. B. Henrich, M. Loparic, F. Safi, A. Eller, W. Halfter, *Exp. Eye Res.* **2013**, *116*, 298.
[32] M. Plodinec, M. Loparic, C. A. Monnier, E. C. Obermann, R. Zanetti-Dallenbach, P. Oertle, J. T. Hyotyla, U. Aebi, M. Bentires-Alj, R. Y. H. Lim, C. A. Schoenenberger, *Nat. Nanotechnol.* **2012**, *7*, 757.
[33] M. Plodinec, M. Loparic, R. Suetterlin, H. Herrmann, U. Aebi, C. A. Schoenenberger, *J. Struct. Biol.* **2011**, *174*, 476.
[34] M. Loparic, D. Wirz, A. U. Daniels, R. Raiteri, M. R. VanLandingham, G. Guex, I. Martin, U. Aebi, M. Stolz, *Biophys. J.* **2010**, *98*, 2731.
[35] D. O. Asgeirsson, P. Oertle, M. Loparic, M. Plodinec, in *Nanoscience and Nanotechnology for Human Health* (Eds: D. O. Asgeirsson, P. Oertle, M. Loparic, M. Plodinec), Wiley, New York **2016**, p. 11.
[36] A. C. Carpenter, R. Bosselut, *Nat. Immunol.* **2010**, *11*, 666.
[37] K. A. Hogquist, Y. Xing, F.-C. Hsu, V. S. Shapiro, *J. Immunol.* **2015**, *195*, 1351.
[38] B. Min, *Front. Immunol.* **2018**, *9*, 547.
[39] J. D. Fontenot, J. P. Rasmussen, L. M. Williams, J. L. Dooley, A. G. Farr, A. Y. Rudensky, *Immunity* **2005**, *22*, 329.
[40] T. Barthlott, A. J. T. Bosch, C. Berkemeier, R. Nogales-Cadenas, L. T. Jeker, M. P. Keller, A. Pascual-Montano, G. A. Holländer, *Eur. J. Immunol.* **2015**, *45*, 1760.
[41] D. H. D. Gray, N. Seach, T. Ueno, M. K. Milton, A. Liston, A. M. Lew, C. C. Goodnow, R. L. Boyd, *Blood* **2006**, *108*, 3777.
[42] I. Yamashita, T. Nagata, T. Tada, T. Nakayama, *Int. Immunol.* **1993**, *5*, 1139.
[43] J. D. Kennedy, C. W. Pierce, J. P. Lake, *J. Immunol.* **1992**, *148*, 1620.
[44] J. Lannes-Vieira, M. Dardenne, W. Savino, *J. Histochem. Cytochem.* **1991**, *39*, 1539.
[45] J. S. P. Ocampo, J. Marques de Brito, E. Corrêa-de-Santana, R. Borojevic, D. M. Serra Villa-Verde, W. Savino, *Cell. Immunol.* **2008**, *254*, 1.
[46] Y. Emre, M. Irla, I. Dunand-Sauthier, R. Ballet, M. Meguenani, S. Jemelin, C. Vesin, W. Reith, B. A. Imhof, *Nat. Commun.* **2013**, *4*, 2842.
[47] P. L. Graney, K. Lai, S. Post, I. Brito, J. Cyster, A. Singh, *Adv. Funct. Mater.* **2020**, *30*, 2001232.
[48] L. E. Wagar, A. Salahudeen, C. M. Constantz, B. S. Wendel, M. M. Lyons, V. Mallajosyula, L. P. Jatt, J. Z. Adamska, L. K. Blum, N. Gupta, K. J. L. Jackson, F. Yang, K. Röltgen, K. M. Roskin, K. M. Blaine, K. D. Meister, I. N. Ahmad, M. Cortese, E. G. Dora, S. N. Tucker, A. I. Sperling, A. Jain, D. Huw Davies, P. L. Felgner, G. B. Hammer, P. S. Kim, W. H. Robinson, S. D. Boyd, C. J. Kuo, M. M. Davis, *Nat. Med.* **2021**, *27*, 125.
[49] C. Bornstein, S. Nevo, A. Giladi, N. Kadouri, M. Pouzolles, F. Gerbe, E. David, A. Machado, A. Chuprin, B. Tóth, O. Goldberg, S. Itzkovitz, N. Taylor, P. Jay, V. S. Zimmermann, J. Abramson, I. Amit, *Nature* **2018**, *559*, 622.
[50] C. N. Miller, I. Proekt, J. von Moltke, K. L. Wells, A. R. Rajpurkar, H. Wang, K. Rattay, I. S. Khan, T. C. Metzger, J. L. Pollack, A. C. Fries, W. W. Lwin, E. J. Wigton, A. V. Parent, B. Kyewski, D. J. Erle, K. A. Hogquist, L. M. Steinmetz, R. M. Locksley, M. S. Anderson, *Nature* **2018**, *559*, 627.
[51] M. A. Asnaghi, T. Smith, I. Martin, D. Wendt, in *Tissue Engineering* (Eds: C. vanBlitterswijk, J. deBoer), Academic Press/Elsevier, Amsterdam, Netherlands **2014**, p. 11.
[52] D. Wendt, A. Marsano, M. Jakob, M. Heberer, I. Martin, *Biotechnol. Bioeng.* **2003**, *84*, 205.
[53] W. Halfter, P. Oertle, C. A. Monnier, L. Camenzind, M. Reyes-Lua, H. Hu, J. Candiello, A. Labilloy, M. Balasubramani, P. B. Henrich, M. Plodinec, *FEBS J.* **2015**, *282*, 4466.
[54] J. E. Sader, I. Larson, P. Mulvaney, L. R. White, *Rev. Sci. Instrum.* **1995**, *66*, 3789.
[55] W. C. Oliver, G. M. Pharr, *J. Mater. Res.* **1992**, *7*, 1564.
[56] M. Plodinec, R. Y. H. Lim, in *Mammary Stem Cells: Methods and Protocols, Methods in Molecular Biology*, Vol. *1293* (Ed: M. Vivanco), Humana Press, New York, NY **2015**.
[57] D. Nečas, P. Klapetek, *Cent. Eur. J. Phys.* **2012**, *10*, 181.